

# Wide-field retinal hemodynamic imaging with the tracking scanning laser ophthalmoscope

**R. Daniel Ferguson and Daniel X. Hammer**

*Physical Science Inc., 20 New England Business Center, Andover MA 01810*  
[ferguson@psicorp.com](mailto:ferguson@psicorp.com), [hammer@psicorp.com](mailto:hammer@psicorp.com)

**Ann E. Elsner, Robert H. Webb, and Stephen A. Burns**

*Schepens Eye Research Institute, Harvard Medical School, 20 Staniford Street, Boston MA 02114*  
[elsner@vision.eri.harvard.edu](mailto:elsner@vision.eri.harvard.edu), [webb@eri.harvard.edu](mailto:webb@eri.harvard.edu), [sburns@vision.eri.harvard.edu](mailto:sburns@vision.eri.harvard.edu)

**John J. Weiter**

*Retinal Specialists of Boston, 100 Charles River Plaza, Boston MA 02114*

**Abstract:** Real time, high-speed image stabilization with a retinal tracking scanning laser ophthalmoscope (TSLO) enables new approaches to established diagnostics. Large frequency range (DC to 19 kHz), wide-field (40-deg) stabilized Doppler flowmetry imaging was demonstrated in initial human subject tests. The fundus imaging method is a quasi-confocal line-scanning laser ophthalmoscope (LSLO). The retinal tracking system uses a confocal reflectometer with a closed loop optical servo system to lock onto features in the ocular fundus and automatically re-lock after blinks. By performing a slow scan with the laser line imager, frequency-resolved retinal perfusion and vascular flow images were obtained free of eye motion artifacts. Normal adult subjects and patients were tested with and without mydriasis to characterize flow imaging performance.

©2004 Optical Society of America

OCIS codes: (000.0000) General.

---

## References and links

1. M. E. Hartnett, J. J. Weiter, G. Staurenghi, and A. E. Elsner, "Deep retinal vascular anomalous complexes in advanced age-related macular degeneration," *Ophthalmol.*, **103**, 2042-2053 (1996).
2. D. Gabor, "Laser speckle and its elimination," *IBM J. Res. Dev.* **14**, 509-514 (1970).
3. J. D. Briers, "The statistics of fluctuating speckle patterns produced by a mixture of moving and stationary scatterers," *Opt. Quant. Electron.* **10**, 364-366 (1978).
4. A. F. Fercher and J. D. Briers, "Flow visualization by means of single-exposure speckle photography," *Opt. Commun.* **37**, 326-329 (1981).
5. J. C. Dainty (ed.), *Laser Speckle and Related Topics*, Vol. 9 in series *Topics in Applied Physics*, Springer-Verlag, Berlin (1975 and 1984).
6. A. E. Ennos, "Speckle interferometry," In: *Laser Speckle and Related Topics*, Vol. 9 in series *Topics in Applied Physics*, Second Edition, pp. 203-253, J. C. Dainty (ed.), Springer-Verlag, Berlin (1984).
7. J. W. Goodman, "Statistical properties of laser speckle patterns," in *Laser Speckle and Related Topics*, J. C. Dainty, ed. (Springer-Verlag, Berlin, Second Edition 1984), pp. 9-75.
8. J. D. Briers, "Speckle fluctuations and biomedical optics: implications and applications," *Opt. Eng.* **32**, 277-283 (1993).
9. R. Bonner and R. Nossal, "Model for laser Doppler measurements of blood flow in tissue," *Appl. Opt.* **20**, 2097-2107 (1981).
10. C. Riva, B. Ross, and G. Benedek, "Laser Doppler measurements of blood flow in capillary tubes and retinal arteries," *Invest. Ophthalmol.* **11**, 936-944 (1972).
11. T. Tanaka, C. Riva, and I. Ben-Sira, "Blood velocity measurements in human retinal vessels," *Science* **186**, 830-832 (1974).
12. H. Fujii, "Visualization of retinal blood flow by laser speckle flowgraphy," *Med. & Biol. Eng. & Comput.* **32**, 302-304 (1994).

13. N. Konishi and H. Fujii, "Real-time visualization of retinal microcirculation by laser flowgraphy," *Opt. Eng.* **34**, 753-757 (1995).
  14. J. D. Briers, G. Richards and X. W. He, "Capillary blood flow monitoring using laser speckle contrast analysis (LASCA)," *J. Biomed. Opt.* **4**, 164-175 (1999).
  15. G. Michelson, B. Schmauss, M.J. Langhans, J. Harazny, M.J.M. Groh, "Principle, validity, and reliability of scanning laser Doppler flowmetry," *J. Glaucoma* **5**, 99-105 (1996).
  16. G. Michelson, J. Welzenbach, I. Pal, J. Harazny, "Functional imaging of the retinal microvasculature by scanning laser Doppler flowmetry," *Int. Ophthalmol.* **23**, 327-335 (2001).
  17. D. Huang, E. A. Swanson, C. P. Lin, J. S. Schuman, W. G. Stinson, W. Chang, M. R. Hee, T. Flotte, K. Gregory, C. A. Puliafito, and J. G. Fujimoto, "Optical Coherence Tomography," *Science* **254**, 1178-1181 (1991).
  18. J. A. Izatt, M. D. Kulkarni, S. Yazdanfar, J. K. Barton, and A. J. Welch, "In vivo bidirectional color Doppler flow imaging of picoliter blood volumes using optical coherence tomography," *Opt. Lett.*, **22**, 1439-1441 (1997).
  19. T. G. van Leeuwen, M. D. Kulkarni, S. Yazdanfar, A. M. Rollins, and J. A. Izatt, "High-flow-velocity and shear-rate imaging by use of color Doppler optical coherence tomography," *Opt. Lett.* **24**, 1584-1586 (1999).
  20. X. J. Wang, T. E. Milner, and J. S. Nelson, "Characterization of fluid flow velocity by optical Doppler tomography," *Opt. Lett.* **20**, 1337-1339 (1995).
  21. S. Yazdanfar, A. M. Rollins, and J. A. Izatt, "Imaging and velocimetry of the human retinal circulation with color Doppler optical coherence tomography," *Opt. Lett.* **25**, 1448-1450 (2000).
  22. B. R. White, M. C. Pierce, N. Nassif, B. Cense, B. H. Park, G. J. Tearney, B. E. Bouma, T. C. Chen, and J. F. de Boer, "In vivo dynamic human retinal blood flow imaging using ultra-high speed spectral domain optical coherence tomography," *Optics Express* **11**, 3490 (2003), <http://www.opticsexpress.org/abstract.cfm?URI=OPEX-11-25-3490>.
  23. D. X. Hammer, R.D. Ferguson, T. Ustun, G. Dadusc, R.H. Webb, "Hand-held digital line-scanning laser ophthalmoscope (LSLO)," in *Ophthalmic Technologies XIV*, F. Manns, P. G. Söderberg, A. Ho, eds., Proc. SPIE **5314**, 161-169 (2004).
  24. R. Daniel Ferguson, "Servo tracking system utilizing phase-sensitive detection of reflectance variation," U.S. Patents #5,767,941 and #5,943,115.
  25. D. X. Hammer, R. D. Ferguson, J. C. Magill, M. A. White, A. E. Elsner, and R. H. Webb, "Image stabilization for scanning laser ophthalmoscopy," *Opt. Express* **10**, 1542-1549 (2002), <http://www.opticsexpress.org/abstract.cfm?URI=OPEX-10-26-1542>.
  26. D. X. Hammer, R. D. Ferguson, J. C. Magill, M. A. White, A. E. Elsner, and R. H. Webb, "Compact scanning laser ophthalmoscope with high speed retinal tracker," *Appl. Opt.* **42**, 4621-4632 (2003).
- 

## 1. Introduction

The retina is among the most highly vascularized and metabolically active tissues in the body. Like the central nervous system of which it is a part, it is also susceptible to ischemic injury. Degenerative diseases of the eye often have either hemodynamic consequences or causes, though many mechanisms remain unknown. Improved blood flow imaging diagnostics for retinal circulation and perfusion will aid the detection and management of eye disease, and research on retinal function and metabolism.

The retinal circulation apparent in images generated by scanning laser ophthalmoscopy (SLO) originates from the central retinal artery that passes through the optic nerve head before branching into superior, inferior, nasal, and temporal arteries, into many smaller vessels, and ultimately, into capillary networks. The underlying choroidal vessels and choriocapillaris beneath the retinal pigment epithelium (RPE) account for nearly 90% of the blood flow in the eye [ref]. While rapid flow in the retinal vascular tree is readily visualized, the perfusion of the retina through the micro-vasculature on both sides of the RPE is critically important. For eye diseases such as diabetic retinopathy, macular degeneration, and glaucoma, these structures will exhibit early flow defects or the growth of new vessels triggered by metabolic distress and other factors [1].

Both the retinal and choroidal vessel diameters range from  $\sim 5 \mu\text{m}$  (in the retinal capillary bed and choriocapillaris) to  $\sim 0.4 \text{ mm}$  (major vessels) [ref]. Flow rates range from local quasi-isotropic perfusion rates of tens of  $\mu\text{m/s}$  in the capillaries to pulsatile values of several  $\text{cm/s}$  in the arteries [ref]. This range of dimensions and flow parameters presents an extremely

demanding diagnostic problem in terms of spatial resolution, field of view, and dynamic range. Fluorescein angiography is a powerful tool for global visualization of retinal vessel topology, occlusions and, uniquely, leakage. However at present, early transit phase angiography can provide at best only a fleeting glimpse of dynamic effects because of the rapidity of fluorescein molecular diffusion. Few methods accomplish dynamic blood flow imaging non-invasively (i.e., without dyes); fewer still quantitatively; and none with the wide field, high resolution, and dynamic range to globally characterize retinal hemodynamics. Reproducibility is essential for longitudinal studies, and also for sensitive detection of functional correlations with local neuronal activity or pharmacological effects. In short, despite decades of research and the introduction of several advanced systems for measurement of blood flow, quantitative retinal blood flow diagnostics have not yet achieved the clinical prominence that retinal biology would seem to justify.

### *1.1 Doppler and speckle imaging*

When imaging biological tissues with lasers, the phenomenon of speckle is a necessary consequence of coherent illumination. The superposition of scattered photons from an extended source produces the net wavefront at the receiving aperture whose amplitude and phase varies rapidly from point to point. This is the source of the large fluctuations in apparent reflectivity and the granularity in captured images. A stationary ensemble of scatterers will produce a stationary speckle pattern. Such variations are not intrinsic reflectivity variations and so from an imaging viewpoint may be regarded as noise, with concomitant reduction of image contrast and spatial resolution. When particles are also in motion, however, the scattered light also has imposed Doppler frequency shifts dependent upon the scattered wave-vectors and the particles' velocities. The frequency content of the imaged light can be measured and velocities inferred. In this sense, in living biological tissue speckle can be regarded as a contrast agent enabling the visualization of dynamic processes [1-8]. **Renumber from here**

Speckle interferometry and its related imaging technologies exploit the temporal characteristics of fluctuations that contain information about the motion of particles within an optically probed or imaged volume. The DC or zero frequency component of the temporal spectrum at an image pixel contains the time-averaged power during the observation, and therefore asymptotically, the intrinsic incoherent reflectivity or the "speckle-free" image. The AC component contains quantitative measures related to particle number density and velocity distributions within the probed volume element (voxel).

Red blood cells are strongly forward scattering in the near infrared and most of the scattered light per interaction falls within a sharply peaked cone with ~6 deg half angle [8]. Mainly, light forward scattered by blood is subsequently backscattered by denser tissues. This enables velocities perpendicular to the incident beam to contribute to the flow signal, but can result in Doppler signals whose origin is ambiguous. At the largest scales of arteries and veins, the velocities are large with a single well-defined direction. However, at the capillary or perfusion scale, velocities are small, perhaps with multiple flow directions within a single voxel. Multiple light scattering can cause these fine scales to lose contrast in the flow images. However, the total Doppler signal power per unit of imaged tissue volume is approximately preserved [8].

The first applications of Doppler methods to retinal blood flow diagnostics were developed by Riva et al. [9,10]. In early work, a single laser beam was focused on the retina, and the flow in retinal vessels and capillary perfusion was found to be measurable and quantifiable with laser Doppler flowmetry. Later, two imaging approaches emerged using CCD fundus images (laser speckle imaging or flowgraphy) [11-13] and flying-spot confocal SLO devices such as scanning laser Doppler flowmetry (e.g. Heidelberg Retinal Flowmeter, HRF) [14,15]. Concurrently, color Doppler optical coherence tomography (OCT) or optical Doppler tomography (ODT) were found to provide local anatomical detail with velocity information when blood moves parallel to the probe beam. Such measurements can be difficult to interpret for complex vessel topology [16-20]. Most recently, the remarkable

capabilities of high-speed, spectral domain ODT (SDODT) for blood flow measurement have been described [21]. The improvement in retinal flow visualization has been considerable. However, all of these approaches trade resolution, field-of-view, dynamic range, velocity component sensitivity and Doppler frequency range against scan speed and system noise. The motion of the eye, the cardiac and respiratory rhythms and other effects render the lowest frequencies virtually uninterpretable. Low data rates and high-frequency aliasing render the highest flows inaccessible and/or inaccurate.

### *1.2 Stabilized Doppler flowmetry (SDF)*

Most scanning imaging technologies suffer from practical limitations in the living eye at eye-safe light levels: scan areas or volumes and scan times are restricted by eye motions or other registration issues which corrupt data and are generally not correctable by post-processing. In other words, at present almost all scanning imaging operations must fit within a relatively brief window in time – typically the order of a second, approximately the mean time between small saccades. This usually severely impacts the size of the measured fields and the trade-offs that must be made in data quality. The resulting difficulties of flow quantification, velocity range, sensitivity, dynamic range, and field of view especially for correlating local flow measures on the retina to the wide-field clinical angiographic picture, have not yet been overcome.

In order to address some of these issues, we have previously combined two technologies, the quasi-confocal line-scanning laser ophthalmoscope [22] and the high-speed retinal tracking system [23] yielding a tracking scanning laser ophthalmoscope (TSLO) [24,25]. In the present investigation, the TSLO is configured for wide-field, large dynamic range stabilized Doppler flowmetry (SDF). Because of the high fidelity retinal tracking function, eye motion artifacts are eliminated. In this way the temporal spectrum at each pixel is obtained. High contrast, low-noise, frequency-resolved retinal microvasculature and perfusion maps are thus visualized in a new dye-free angiography mode. With this novel imaging approach and advanced user interface features, the accessible Doppler frequency range for blood flow has been significantly expanded both upwards and downwards, while eliminating confounding imaging artifacts and some limitations of earlier methods.

At first sight, the addition of real time, high-speed retinal image stabilization appears merely to be a convenience. While retinal tracking certainly simplifies some current clinical diagnostic protocols, and virtually eliminates registration issues by stabilizing relative to fixed retinal landmarks, its real contribution is potentially more fundamental. Tracking enables the duration of any given scan or scan sequence to be effectively indefinite. The familiar continuous scan dimensions are the A-scan (z axis), B-scan (x-axis), and C-scan (y-axis). Precision stabilization robustly adds a new scan dimension to clinically practical diagnostics: the T-scan (the time axis).

## **2. Materials and Methods**

The TSLO served as the platform for the SDF blood flow experiments and has been described in detail elsewhere [24,25]. A 25- $\mu$ W, 880-nm LED tracking beam is dithered on a retinal feature – usually the lamina cribrosa in the optic nerve head – and detected with a confocal reflectometer. The processed reflectance signals were used to create error signals proportional to eye movements and fed back to an *x-y* galvanometer-driven mirror pair. A 300- $\mu$ W, 780-nm laser illumination beam was fanned out on the retina and detected with a linear image sensor. The videos presented in this paper were acquired with a linear detector with a line rate of 7.5k lines/sec (Physical Sciences Inc.), which precluded measurement of the peak velocity but allowed for higher resolution images of retinal perfusion. An alternate image sensor with a line rate up to 39k lines/sec (Fairchild Imaging Inc.) was also used to measure peak arterial velocity. In the conventional scanning mode, the line is swept over the retina at a rate that can exceed 60 frames/sec. An algorithm has been implemented to automatically re-lock the system after subject blinks. Figure 1 shows a video and position signals during tracking and re-lock through blinks.

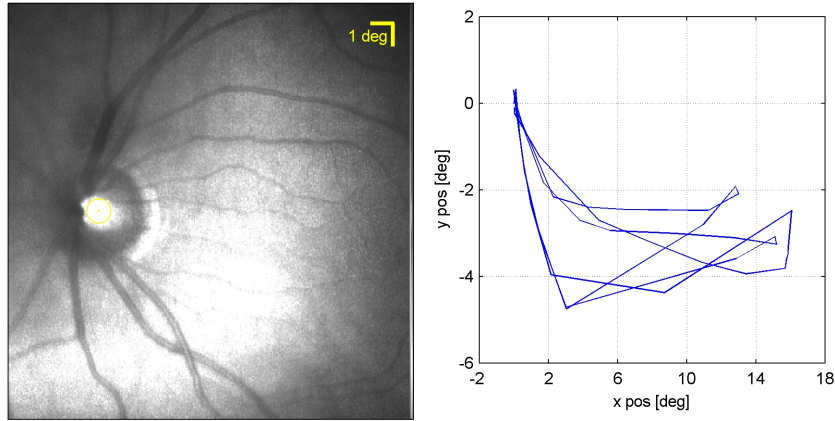


Fig. 1. (2.3 MB) Video and x-y eye positions during automatic re-lock after blinks.

The SDF technique introduces a new, fast, and efficient approach to blood flow image capture. By performing slow infrared line scans, tracking the eye and re-locking after blinks, frequency-resolved images of retinal flow are obtained. Figure 2 illustrates the technique in comparison to the HRF. The linear array is read out 512 times at one line on the retina and stored as a single BT image plane (i.e., x-line vs. time) before the next line is scanned. Each BT plane of the image cube therefore comprises an image of 512 spatial pixels by 512 or more temporal pixels. Since the linear sensor integrates the light collected from each line, a continuous temporal profile is obtained for the duration of the BT scan. In a slow C-scan, 512 such BT planes are captured across the fundus, taking up to 30 seconds to complete a full BTC image cube. Two scans in immediate succession (1 minute) are now routinely performed, so that blanking that occurs during blinks can be overwritten by the valid data of the twin scan. Scans can be precisely repeated after any intervening interval by simply locking onto the same retinal feature.

After image cube acquisition, a fast Fourier transform (FFT) was applied to extract the full power spectrum at each image pixel. The frequency spectra were normalized by the DC value to remove intensity reflectance variation across the image. To create frequency videos, the spectra at each pixel were binned with several different windows, including one with a fixed size and one with octave increments (2,4,8...). The most common processing shown in the videos presented herein, used an overlapping moving window with an increment and halfwidth of 8 and 16 frames (117 and 234 Hz for the PSI camera), respectively. After binning, the individual frequency frames were contrast-stretched. The processing takes less than 3 minutes with a 1.8-GHz Pentium IV processor.

In contrast to SDF with the TSLO, the HRF samples each pixel of each line at a rate of 4k lines/sec (Fig. 2b). A significant impact of this lower line rate – determined by the mechanical hardware – is that the Nyquist Theorem limits the maximum frequency detected to 2 kHz. Even more important is the fact that the duty cycle will be an extremely small percentage (1/256) contingent upon the number of pixels in the line. This detection approach based upon sampling leads to aliasing and consequently, velocity errors. Moreover, since tracking is not employed in the HRF, frequencies below 125 Hz are disrupted by motion and not processed or displayed. Eye motion also prevents acquisition of even moderately-sized and sampled retinal fields. The BTC scan dimensions of the HRF are 256×126×64, 64 times smaller and up to 10 times slower than the TSLO with scan dimensions of 512×512×512.

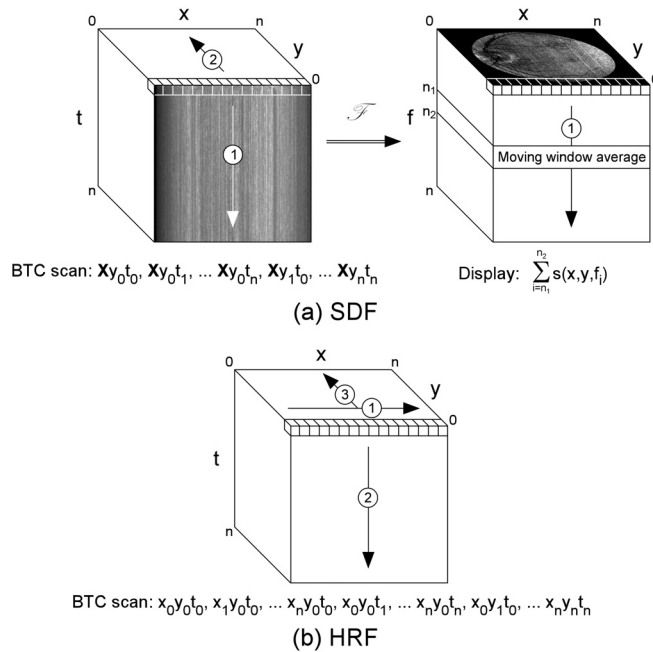


Fig. 2. Diagram illustrating the slow scan technique for SDF (a) and for the HRF (b). The order of the BTC scan sequence is numbered on the diagram. The scan equation is shown below the diagram for each type. After Fourier transformation, the data cube is displayed as a video where individual frames are created by binning individual frequencies with a moving window.

### 3. Results

We utilized the TSLO in SDF mode for wide-field blood flow imaging and have performed SDF scans in seven normal subjects and four retina patients. Videos created from two normal subjects and two retina patients are shown in Figs. 3-5 and 7. The first frame of each video is the reconstructed fundus image created from the DC value. The videos are displayed at 10 frames/sec but each frequency bin can be viewed by stepping through frames in Windows Media Player or Apple Quicktime.

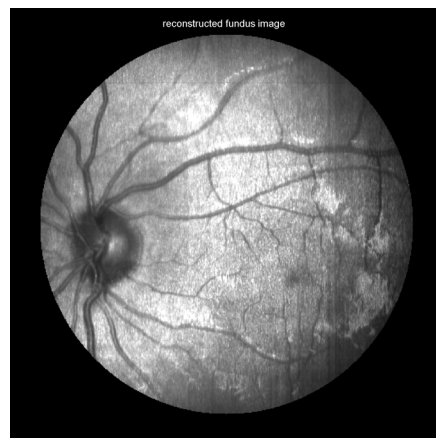


Fig. 3. (2.0 MB) Reconstructed image and blood flow video for a healthy 24 year old subject.

Figure 3 shows the blood flow video for a healthy 24-year old subject. The vertical lines at the lowest frequency bin are caused by small amplitude (1 pixel) transient tracking stability artifacts due to nystagmus invoked by occasional fixation on the scanning line as it passes across the fovea. The foveal avascular region is also clearly visible at low frequencies. In the lower frequency bins ( $f < 400$  Hz), or the “perfusion range”, flow in the retinal capillary beds and the choriocapillaris creates a bright field that is shadowed by the overlying retinal vessels, which happen to be dark in these frequency bins. This implies that the choroidal contribution to the flow maps can be attenuated by the RPE in darkly pigmented eyes, and perhaps by the focus and depth of field of the quasi-confocal imaging system. In middle frequency bins ( $f = 400 - 1000$  Hz), very small retinal vessels emerge, as well as pronounced peripapillary flow. At the highest frequencies ( $f > 1000$  Hz), the small vessels gradually fade and only the signal from the largest vessels in the retina and choroid can be detected. Note also the change in the reflectance of the lamina cribrosa as the frequency increases.

A normal subject with lighter pigmentation shows much more choroidal flow detail in Figure 4. This subject was highly myopic accounting for the larger variation in focus across the field in the reconstructed fundus image. The foveal avascular region is again apparent at lower frequencies. At higher frequencies, vertical banding caused by pulsatile flow is quite strong in this subject in the choroid visible below the retinal circulation. It is interesting to observe that very little of this pronounced choroidal structure is visible in the reconstructed SLO image. The perfusion of the choriocapillaris is undoubtedly contributing to the perfusion maps, but it does not overwhelm the retinal signal.

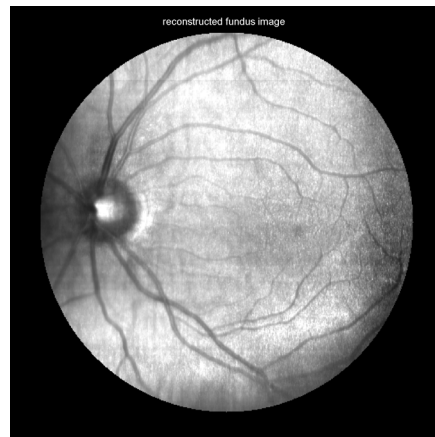


Fig. 4. (2.2 MB) Reconstructed image and blood flow video for normal subject with light pigmentation.

A retina patient shows signs of local perfusion defects associated with central serous chorioretinopathy in the reconstructed fundus images in Figure 5. However, perfusion appears to be normal in the low frequency frames of the video. Choroidal flow was difficult to observe but visualization of medium-sized vessels at middle frequencies was more pronounced in this darkly pigmented eye.



Fig. 5. (2.2 MB) Reconstructed image and blood flow video for retina patient.

In the same patient, a higher-frequency (19 kHz), higher-magnification scan was acquired to determine the peak of laminar Poiseuille flow in the larger retinal arteries (Figure 6). The average flow edge (FWHM) for a small section of artery was measured at each frequency bin and the resultant data fit to a parabolic profile. At frequencies greater than 6 kHz, the flow signal was confined to a region smaller than the approximate resolution of the imaging system ( $\sim 40 \mu\text{m}$  on the retina) and no further decrease in diameter was seen. The fit corresponds well with the maximum resolvable frequency in the video ( $\sim 8 \text{ kHz}$ ) and with previous reported measurements [ref Riva Applied Optics].

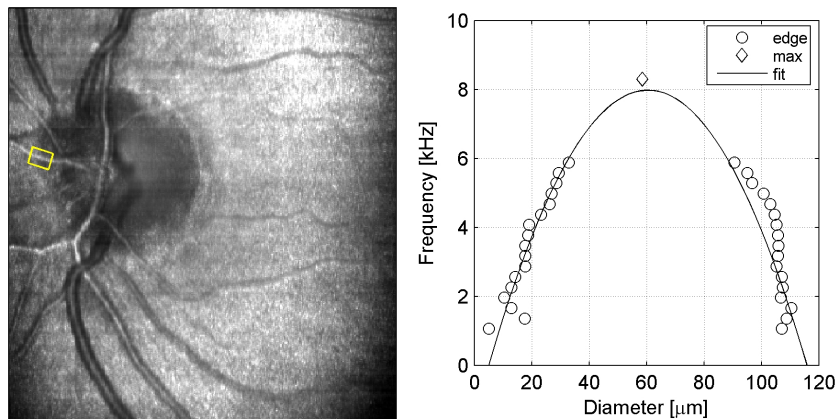


Fig. 6. Laminar Poiseuille flow measured in a major retinal artery (indicated by yellow box) from a high-frequency, high-magnification scan. The FWHM vessel edges (circles) are plotted and fit to a parabolic curve. The frequency of flow in the vessel is indicated up to the measured resolution limit of the imaging system. The maximum detectable frequency is also indicated (diamond).

Figure 7 shows the blood flow video from a 68-year old patient with macular degeneration. Perfusion anomalies associated with apparent pathology are evident in the low frequency images, but also a large area of reduced perfusion temporally. At present these effects are difficult to categorize and interpret. The binned images show significant detail, even though the DC fundus image is not optimally focused through the relatively optically poor ocular media in this subject. Middle frequency peripapillary flow signal that was evident in all (younger) normal subjects was not visible in this patient.

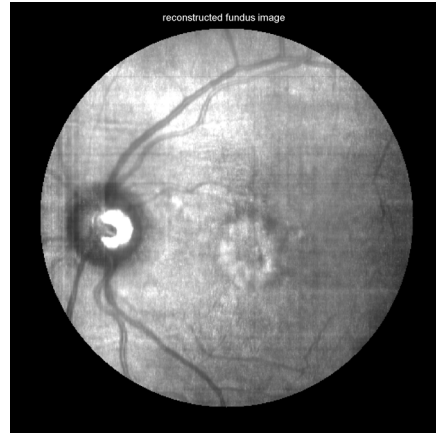


Fig. 7. (2.3 MB) Reconstructed image and blood flow video for macular degeneration patient showing reduced perfusion in the macula.

Figure 8 illustrates an alternate representation of blood flow information with false color maps. To generate these maps, the transformed videos were averaged into three arbitrarily chosen bins roughly representing the perfusion ( $f < 400$  Hz), middle flow ( $f = 400 - 1000$  Hz), and high flow ( $f > 1000$  Hz) ranges. The three bins were then mapped into RGB colors, normalized, and displayed. Two different normalization techniques were employed. The first, shown in the upper row of Fig. 8, was to normalize each color plane individually so that the overall intensity range of each flow bin was matched in the composite image. This creates a white pixel at a point where flow was roughly equally distributed across the spectrum and a black pixel where no flow at any frequency was present. Where high or low flow dominated, the pixel is more blue or red. The second normalization technique is shown in the lower row of Fig. 8. It normalized all color planes to the power per frequency bin. In this representation, the overall map color will be determined by which flow region dominated. Thus, the first normalization scheme can be used to compare structures within an image but not from subject-to-subject because the normalization is relative, whereas the second normalization scheme can be used to make comparisons between subjects.

Figure 8 was created with data from the second normal subject and the retinal subjects presented previously. In the lightly pigmented subject, the higher choroidal flow (blue) is apparent in the nasal portion of Fig 8a. In the retina patient with higher pigmentation, medium flow retinal vessels (green) are dominant (Fig. 8b). In both retina patients, the high pulsatile flow is also visible (Fig. 8b and c). In subjects with global blood flow defects, changes visualized with the second normalization technique are dramatic compared to those without defect (Fig. 8d-f).

#### 4. Discussion

The partitioning of the flowmetry data into normalized frequency bins, which divides the images by vessel size and/or flow rate, is only useful with the low noise levels achieved with the SDF scans. The sharpness of the reconstructed DC fundus images is evidence of tracking fidelity during the long scans. The perfusion images ( $f < 400$  Hz) have similar appearance and correspond to the Doppler velocities,  $v < 125 \mu\text{m/s}$ , where  $f \propto vn/\lambda$ , and  $n$  is the refractive index, without reference to flow direction. These images combine retinal and choroidal contributions.

The remaining bins begin to reveal the various vessel size and flow speed echelons in the vascular tree, up to velocity component values of  $\sim 2$  mm/s. The forward scattering angle through the blood in the in-plane velocity in the larger vessels means that the actual flow velocities may be several times higher. In a large superficial retinal artery, we used a sensor with a maximum line rate of 39k lines/sec to measure laminar Poiseuille flow and a peak

velocity of  $\sim 5$  mm/s. Depending on pigmentation and pathology, the larger vessels and highly pulsatile flow of the choroid can be clearly seen in some eyes, but less well in others.

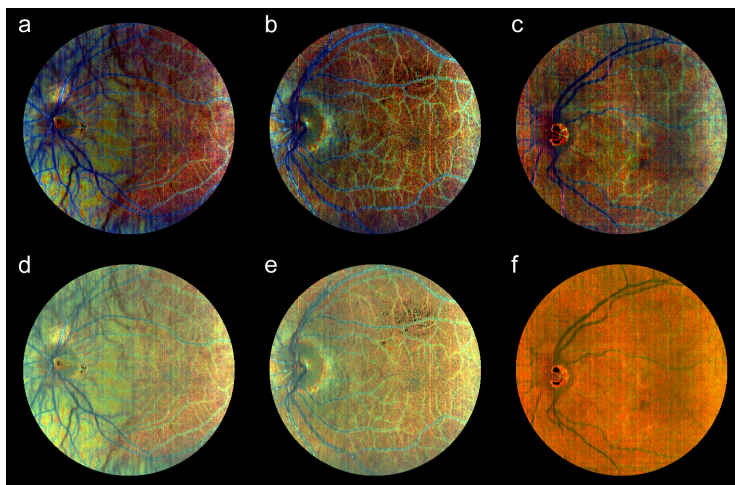


Fig. 8. False color composite blood flow images for second normal subject (a,d) and both retina patients (b,c,e,f). Upper row (a-c) shows images created with individually normalized frequencies bins and lower row shows images created when the composite image was normalized to the power in each bin.

The current approach provides whole retina information by taking advantage of the relatively large depth of field of the SDF (TSLO) optical system ( $\sim 1$  mm) and the fact that the line scanning system is only quasi-confocal and does not possess the full intrinsic sectioning capability of purely confocal flying spot scanning systems. While this mixes information from the choroid and retina, especially at low flow rates, it allows a single data set to be generated to characterize global ocular health. Alternate modes are possible to provide finer depth sectioning of the vasculature including stereo imaging with a dual detector and split pupil or low-coherence imaging techniques. These capability are being evaluated with the TSLO, but have not yet been applied to SDF scans.

Future work will include additional clinical testing, development of higher dynamic range systems, improved depth resolution, and cardiac synchronization for wide-field pulsatile flow characterization. The large dynamic range available with SDF will be used with higher magnification imaging to validate improved quantitative blood flow analysis methods, and to characterize local perfusion defects or neovascular growth.

#### **Acknowledgments**

This work was supported by NIH Grants EY11577 and EY14375, and Physical Sciences Inc. The authors thank Scott Meyer for helpful discussions.